Journal of the Physical Society of Japan
Vol. 52, No. 6, June, 1983, pp. 2210–2215

Spin-Wave Dispersion in $KFeS_2$—a Linear Chain Antiferromagnet and a Spin Analogue of Two Iron Ferrodoxins—by Neutron Inelastic Scattering

Masakazu NISHI, Yuji ITO and Satoru FUNAHASHI†

Institute for Solid State Physics, University of Tokyo, Roppongi, Minato-ku, Tokyo 106
†Physics Division, Japan Atomic Energy Research Institute, Tokai, Ibaraki 319-11

(Received February 7, 1983)

Inelastic neutron scattering has been used to study the magnetic excitation spectrum of $KFeS_2$—a spin analogue of the oxidized two iron ferredoxins—in the antiferromagnetically ordered state. The observed spin wave dispersion relations along a*, b*, c* directions at 77 K are analyzed to give the nearest neighbor intra-chain exchange constant $J_1=-168.1\pm4.8$ cm^{-1} (-20.84 ± 0.60 meV), and the ratio of the nearest interchain to the intra-chain interaction $|J_3|/|J_1|=8.6\times10^{-3}$ indicative of the strong covalency and of the one-dimensional character of the interaction. The anisotropy field of 6040 ± 91 Oe obtained from the gap at the zone center results mostly from the non-dipolar energy. A contribution of quartic terms of spins in the anisotropy energy is needed to account for the observed easy spin direction.

§1. Introduction

The iron of $KFeS_2$ is surrounded by 4 sulfur atoms forming a slightly distorted tetrahedron whose corner is shared by the next iron atom along the c-axis. Such an iron-sulfur cluster is commonly found in units of one to four in the iron-sulfur proteins called ferredoxins which play important roles in the biochemical oxidation reduction electron transport processes.

Although in $KFeS_2$, the FeS_2 clusters repeat in every two units along the c-axis making a linear chain, the local bond configuration of the two repeating units resembles closely to that of 2Fe-oxidized ferredoxin,[1] for example, of Spirulina platensis as evidenced by the recent determination of X-ray crystallography.[2] In the oxidized state of the two iron ferredoxins, the two irons are believed to be antiferromagnetically coupled, and so is the iron in the $KFeS_2$ chain as we reported previously.[3] These observations indicate the close similarity in the electronic structure of Fe in both $KFeS_2$ and the 2Fe-oxidized ferredoxin, and further studies of the iron-iron interaction in $KFeS_2$ are important in understanding the nature of the electronic states of the iron-sulfur cluster.

Such studies are also interesting from the view point of the spin dynamics, since the moment value determined by the previous neutron diffraction work is reduced to about a half of what is expected to the Fe^{3+} indicative of a strong covalency. So far very little work of spin dynamics has been done with compounds having such strong covalent effect.

We report here the magnon dispersion in $KFeS_2$ measured by the neutron inelastic scattering with the purpose to clarify further the electronic states of the iron in the linked cluster of FeS_4 tetrahedra.

§2. Experimental Details

$KFeS_2$ crystallizes in a monoclinic structure C_{2h}^6-$C2/c$ with the cell dimensions of $a=7.09$ Å, $b=11.27$ Å, $c=5.39$ Å with $\beta=113.2°$ at R.T. and includes four formula units per unit cell.[4] The atomic positions are shown schematically in Fig. 1(a). The Néel temperature is 250.0 K and the magnetic structure below T_N is also illustrated in Fig. 1(b).

Single crystals were grown by the Bridgman method from the polycrystal samples which

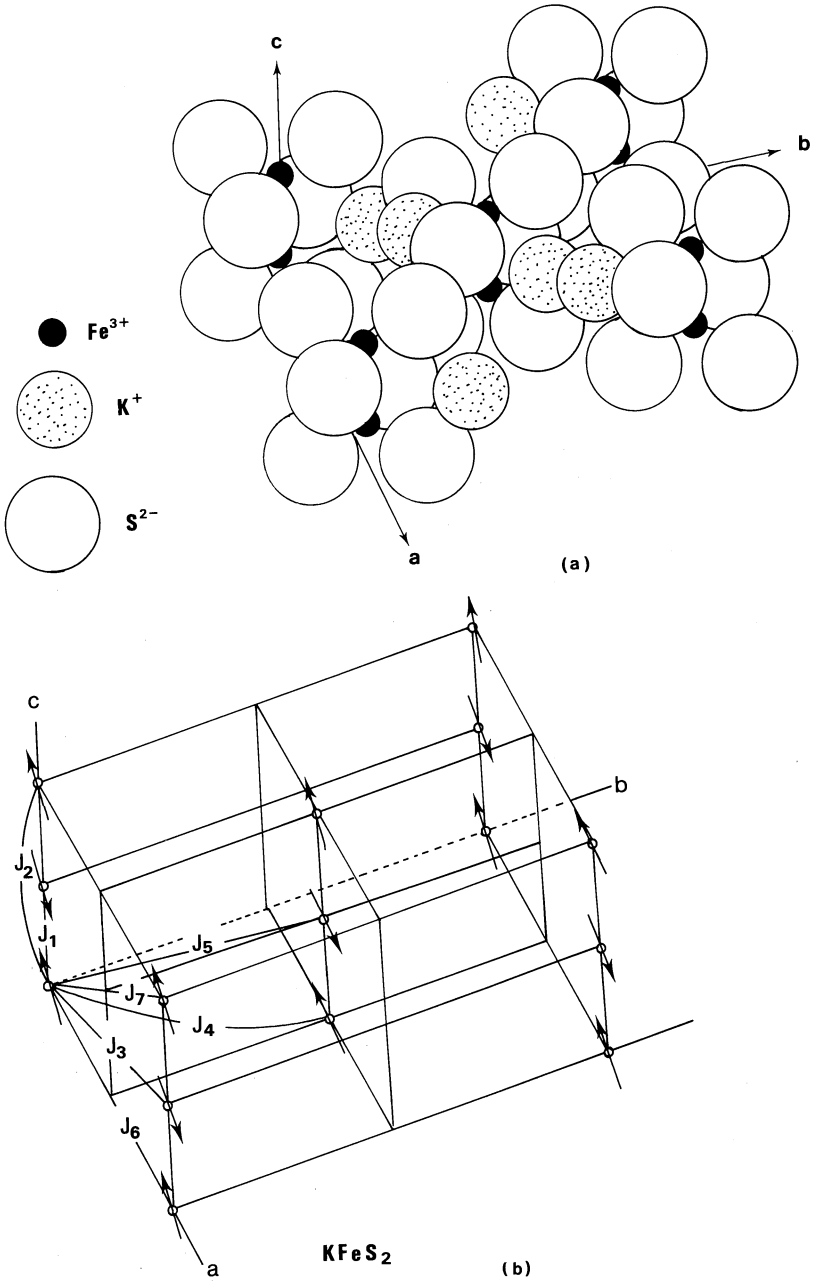

Fig. 1. A schematic illustration of the crystal structure of $KFeS_2$ is shown in (a), and the antiferromagnetic structure is depicted in (b).

were prepared separately by fusing iron powder with sulfur in the presence of anhydrous sodium and potassium carbonate. The single crystals grow in rodlike shapes in which the *c*-axis lies in the longer direction. The one used in the present neutron investigation is ellipsoidal in shape with 1.6 cm in length and 1.6 cm in diameter with relatively large mosaic spread of about 1.5 degrees. The sample was oriented with *a*-axis upright so that [010] and [001] directions were in the scattering plane. For the measurement of the dispersion along a^*-direction, we set the *b*-axis along the sample goniometer axis.

Preliminary measurements soon revealed that the magnon energies were rather large for all three directions, and especially so along the c^*-direction, which necessitated the use of high incident neutron energy. This combined with the large sample mosaic spread means relatively poor energy resolution for the results. The lack of the energy resolution as well as of the anisotropy in the measured susceptibility near and above T_N justified the assumption that the spin wave dispersion of the two sublattices would be degenerate in the absence of the external field, and we only tried the measurement for the so-called AF magnetic zone.

The measurements were performed using three different spectrometers, PANSI and ND-1 of ISSP, CTNS of JAERI all situated at JRR-2 reactor of JAERI, Tokai, Ibaraki. Scans were made all in the constant Q mode with the incident neutron energy from the (002) reflection from PG monochromator fixed at predetermined values depending on the run. Except for 13.7 meV and 41.0 meV incident neutron energies for which a PG filter was used, no higher order contaminations in the incident beam were removed for lack of appropriate filters. The collimation was relaxed and mostly 40′ collimations were used throughout. All the measurements were taken at two different temperatures, 77 K and 150 K. Between the two, very little difference in the behaviour of the dispersion was observed.

§3. Experimental Results

Examples of the observed spin wave intensities at $\zeta=0.08$ (ζ: the reduced wave vector) from the magnetic Bragg positions (001) and (003) along c^*-direction at 77 K are shown in Fig. 2. The incident neutron energy E_i of 80 meV was used for this case. The apparent peak position shifts towards the higher energy value as the scattering vector Q increases. This was confirmed to be due to the resolution effect by convoluting the large resolution ellipsoid with the steep spin wave dispersion surface along c^*-direction indicative of the strongly coupled intra-chain iron atoms. The calculation of neutron intensity with the assumed dispersion relation showed

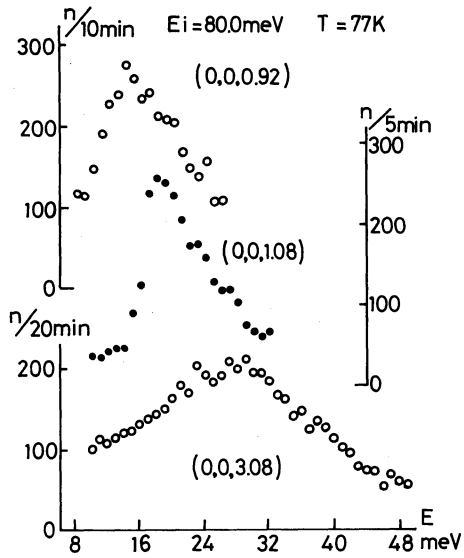

Fig. 2. Examples of the observed spin wave profiles at $\zeta=0.08$ from the magnetic Bragg positions (001) and (003) along c^*-direction at 77 K. All of these correspond to the same spin wave excitation spectrum. The peak position of the one observed at a larger Q value is closer to the true spin wave energy as explained in the text.

that the peak position observed at a larger Q value is closer to the true spin wave energy than that measured at the smaller Q. The observed energy widths can be accounted for by the instrumental resolution including the sample mosaic spread, which was also checked by using the vanadium sample as calibration.

The results of the observed dispersion curve are shown in Fig. 3 along b^*-direction in 3(a), a^*-direction in 3(b) and c^*-direction in 3(c). It should be noticed that the zone boundaries for b^*, c^*-directions are at $\zeta=1.0$ and 0.5 respectively, whereas for a^*-direction it is at $\zeta=0.67$. At the reduced wave vector of $\zeta=1.0$ along the a^*-axis, the energy of the spin wave should coincide with that along the b^*-axis at $\zeta=1.0$ from the symmetry argument, which was indeed the case as shown in Fig. 3. Because of the steep dispersion, we could only observe the magnons along the c^*-direction up to $\zeta=0.14$ at the energy of 40 meV using the incident neutron energy of 80.0 meV.

The observed points indicated in Fig. 3 are obtained after the proper resolution considerations were taken into account. The vertical bars indicate the measure of the half

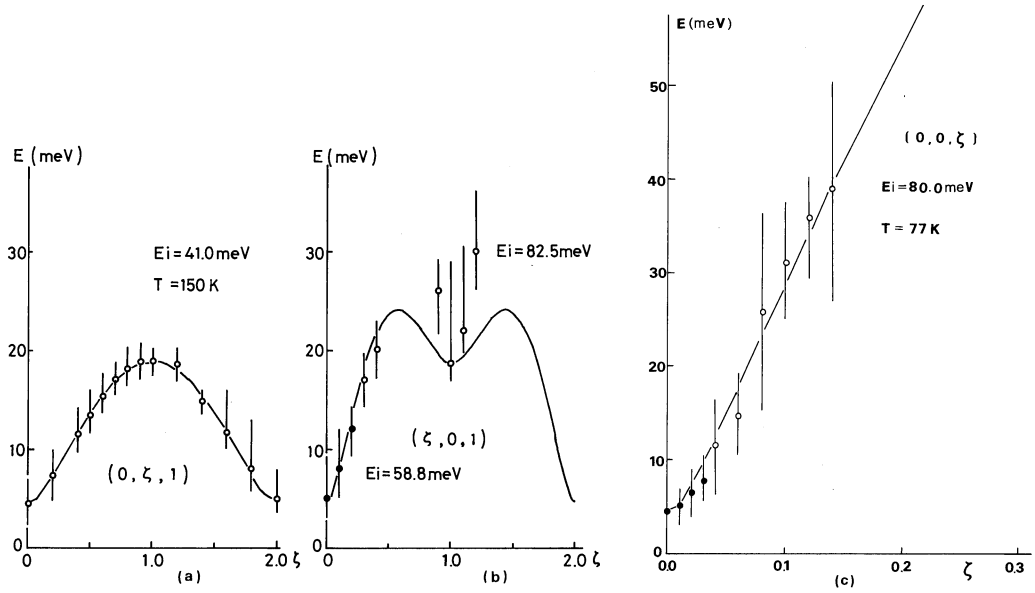

Fig. 3. Spin wave dispersion curves along b^* (a), a^* (b), c^* (c) directions respectively. Bars in the figure represents the measure of the observed half width which comes mostly from the instrumental resolution broadening. Black points at small q indicate that they were taken with the incident energy $E_i = 58.8$ meV, whereas white points were taken mostly with the respective E_i value given in the figure.

width of the observed magnon peaks, which is mostly due to the instrumental resolution broadening as explained above.

§4. Discussion

It is clear from the dispersion relation in Fig. 3, that there is a gap of 4.5 meV at Γ point. In view of this, we take the usual isotropic Heisenberg exchange and the anisotropy field H_A for the Hamiltonian responsible for the observed dispersion,

$$H = -\sum_{i,j} J_j S_i S_{i+j} - g\mu_B H_A \sum_m S_m^z + g\mu_B H_A \sum_n S_n^z, \quad (1)$$

where i numerates the Fe^{3+} sites and j specifies the relevant neighbors. The indices m, n run over the respective sublattice only. The z-axis here corresponds to the ordered spin direction, which is not along the crystallographic axis. The exchange model parameters J_j out to the 7th nearest neighbor are indicated in Fig. 1(b), and their distances are given in Table I, together with the results for J_j and H_A obtained from the analysis.

Since the most complete dispersion curve was obtained along b^*-direction, we first least squares fitted the dispersion along the b^* with the theoretical relation derived from the Hamiltonian (1), in which J_1, J_3, J_4, J_5 and H_A were the necessary parameters for the fitting. It was concluded from this analysis that $|J_4| \cong |J_5|$ was indeed the case as suggested from the same distances from the iron to these 4th and 5th neighbors. We therefore put $J_5 = -J_4$ in the subsequent analysis.

We also put $J_j = 0$ for $j \geq 6$, since the J_4

Table I. Distances and numbers of atoms to the respective nearest neighbors are listed together with the corresponding exchange parameter and the anisotropy field values determined from model fits to the observed dispersion curves.

n.n. No.	r_j(Å)	No. of atoms.	J_j & H_A	Value (meV)*
1	2.70	2	J_1	-20.84 ± 0.60
2	5.40	2	J_2	**
3	6.51	2	J_3	-0.18 ± 0.13
4	6.65	4	J_4	0.094 ± 0.008
5	6.65	4	J_5	-0.094 ± 0.008
6	7.05	2	J_6	$\simeq 0$
7	7.05	2	J_7	$\simeq 0$
—	—	—	H_A	6040 ± 91 Oe

* The unit for H_A is given in Oe in the table.
** The value for J_2 is not required for the fitting and is undetermined as explained in the text.

(and J_5) was already quite small, more than two orders of magnitude less than J_1. The parameter J_2 which represents the ferromagnetic coupling between the 2nd nearest neighbor along the chain (c-axis) direction, comes in only for the dispersion along c^*-direction in the present analysis. However because of the very steep dispersion along c^*, magnon peaks were observed only up to $\zeta=0.14$ under the present experimental condition, and J_2 was not required to improve the fitting in any essential way.

Therefore in the final analysis of the data, the fitting parameters are restricted to the following four. They are J_1, the intra-chain nearest neighbor exchange between iron atoms; J_3 the inter-chain exchange between the nearest neighbor iron atoms along the a-axis; J_4, the exchange parameter for the inter-chain n.n. iron atoms which lie at the face center of the a-b plane; and the energy of the anisotropy field H_A.

The best fitted values for these are given in Table I, and the solid curves in Fig. 3 represent the fitting using these parameters. In deriving these numbers, we used $g=2.03$ determined by EPR in ref. 1 and also by ourselves, and $S=1.17$ at 77 K determined by our previous neutron diffraction work.[3] The ratio of the intra-chain coupling constant to that of the nearest inter-chain is 8.6×10^{-3} indicating a one-dimensional character of the interaction in $KFeS_2$.

The fitting is not so satisfactory along the a^*-axis. We believe the discrepancy near $\zeta=1.0$ along a^* is due to the incomplete resolution correction caused by the poor energy resolution of the raw data rather than the inappropriateness of the fitting procedure.

The value of the intra-chain nearest neighbor coupling constant thus obtained as $J_1=-168$ cm^{-1} (-20.84 meV) should be compared with that of the oxidized spinach ferrodoxin of $J=-183$ cm^{-1} (-22.7 meV) determined from the magnetic susceptibility measurement.[5] A rather good agreement of these values confirms $KFeS_2$ as being a spin analogue compound for the active site of the 2Fe-oxidized ferredoxin, and lends support for the similar electronic structure for the FeS_2 cluster of these two substances.

The magnitude of the intra-chain nearest neighbor iron-iron exchange constant of 20.8 meV ($=168$ cm^{-1}) should also be compared with the ferromagnetic exchange of the pure iron ($J=15.6$ meV) calculated from the spin wave stiffness constant ($D=281$ meVÅ^2)[6] assuming the nearest neighbor interaction only. The observed large exchange constant for $KFeS_2$ even compared to the metallic iron supports the strong covalency of the iron-sulfur bonding in this substance.

The origin of the observed anisotropy field of 6040 Oe cannot be attributed to the dipole-dipole interaction as was done for MnF_2.[7] This is directly demonstrated by calculating the anisotropy energy of the dipole interaction. The results of the computer calculation of the dipole lattice sum for $KFeS_2$ in the antiferromagnetic state are shown in Fig. 4, where the interaction energy is plotted as a function of spin direction with respect to the b-axis. In the figure, θ represents the angle from the c-axis in the a-c plane, and φ the angle from the b-axis in the a^*-b^* plane. The calculation shows if the dipole interaction is the dominant contribution to the magnetic anisotropy of $KFeS_2$, the easy spin direction should be perpendicular to the c-direction pointing towards b-axis. This is in contradiction to the observed spin direction, in which spins are aligned about 13.6° tilted in the a-c plane from the c-axis towards the negative a-direction.[3]

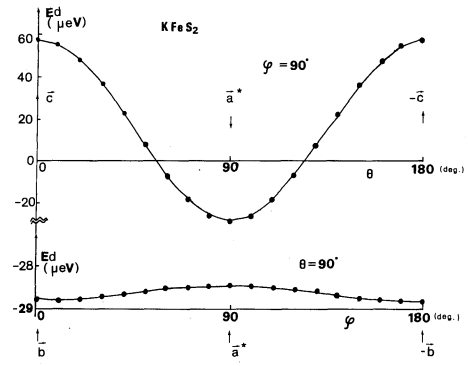

Fig. 4. Dipole lattice sum for spins in the antiferromagnetic state of $KFeS_2$ is plotted (in μeV) as a function of the spin angle. θ represents the angle from c-axis in the a-c plane, and φ, the angle from the b-axis in the a^*-b^* plane. The corresponding crystallographic and the reciprocal axes are also indicated in the figure.

In order to have the spin directed in such a direction in the observed anisotropy field, non-dipolar anisotropy energies of the order of 0.15 meV are needed, which include terms of S_i up to the quartic order either of the single ion crystalline field or of the pseudo-quadrupole interaction form. Such non-dipolar higher order contribution to the anisotropy reflects the strong covalency as well as the low symmetry of the Fe^{3+} site in $KFeS_2$.

Acknowledgements

The authors would like to express their gratitude to Professor K. Hirakawa for many useful discussions.

References

1) W. V. Sweeney and R. E. Coffman: Biochim. Biophys. Acta **286** (1972) 26.
2) T. Tsukihara, K. Fukuyama, M. Nakamura, Y. Katsube, N. Tanaka, M. Kakudo, K. Wada, T. Hase and H. Matsubara: J. Biochem. **90** (1981) 1763, and also by private communication from T. Tsukihara.
3) M. Nishi and Y. Ito: Solid State Commun. **30** (1979) 571.
4) V. W. Bronger: Z. Anorg. Allg. Chemie **359** (1968) 225.
5) G. Palmer, W. R. Dunham, J. A. Fee, R. H. Sands, T. Iizuka and T. Yonetani: Biochim. Biophys. Acta **245** (1971) 201.
6) G. Shirane, V. J. Minkievicz and R. Nathans: J. Appl. Phys. **39** (1968) 383.
7) F. Keffer: Phys. Rev. **87** (1952) 608.